Int. J. Electrochem. Sci., 16 **(2021)** Article Number: 211040, doi: 10.20964/2021.10.57

International Journal of
ELECTROCHEMICAL
SCIENCE
www.electrochemsci.org

Palladium Nanoparticles Supported on Phosphorus-Doped Graphitic Carbon Nitride/Carbon Black Hybrids for Formic Acid Electro-Oxidation

Duo Yu[1,2], Chenxi Lu[1,2], Zhiguo Yan[1,2], Xiaojun Yang[1,2], Wei Yang[1,4,], Zaosheng Lv[3], Zhengfang Tian[5,*] and Qifeng Tian[1,2,*]*

[1] Key Laboratory of Green Chemical Process of Ministry of Education & Hubei Key Laboratory of Novel Reactor and Green Chemical Technology (Wuhan Institute of Technology), Wuhan 430205, People's Republic of China
[2] School of Chemical Engineering and Pharmacy, Wuhan Institute of Technology, Wuhan 430205, People's Republic of China
[3] Key Laboratory of Hubei Province for Coal Conversion and New Carbon Materials, Wuhan University of Science and Technology, Wuhan 430081, People's Republic of China
[4] School of Chemistry and Environmental Engineering, Wuhan Institute of Technology, Wuhan 430205, People's Republic of China
[5] College of Chemistry and Chemical Engineering, Hubei Key Laboratory for Processing and Application of Catalytic Materials, Huanggang Normal University, Huanggang 438000, People's Republic of China
[*]E-mail: qftian@wit.edu.cn (Q. T.), yangweight@126.com (W. Y.), tzf7801@163.com (Z. T.)

Received: 6 July 2021 / *Accepted:* 14 August 2021 / *Published:* 10 September 2021

A novel hybrid supports consisting of phosphorus-doped graphitic carbon nitride and carbon black were prepared for loading Pd nanoparticles (NPs). The obtained Pd/C-PCN catalysts exhibited superior catalytic performance towards formic acid electro-oxidation (FAO). The anchoring effect of the graphite carbon nitride (g-C_3N_4) improved the dispersibility of Pd NPs. It is found that the Pd NPs with a reduced average diameter dispersed on g-C_3N_4 supports compared to that on carbon black. After doping with phosphorus, the prepared Pd/C-PCN-X catalysts has a further improvement in the activity and durability of FAO. Pd/C-PCN-0.2 shows the highest peak current density for FAO. Its peak current density reached 771 A/g, which is 2.15 times that of Pd/C (358 A/g). It also exhibited the best stability for FAO. The enhanced catalytic performances of this Pd/C-PCN-X catalysts can be attributed to high dispersion of Pd NPs and improved electronic structure of Pd NPs caused by P doping.

Keywords: carbon nitride; phosphorus-doped; palladium; formic acid oxidation; electrocatalysis

1. INTRODUCTION

Due to the rapidly increasing energy demand and limited access to natural fossil fuels, the development of sustainable and renewable power sources is receiving widespread attention[1]. Fuel cells are green energy sources and can replace fossil fuels. In recent years, direct formic acid fuel cells (DFAFC) have attracted the attention of the scientific community due to their unique advantages over hydrogen fuel cells and direct methanol fuel cells (DMFCs)[2]. For hydrogen fuel cells, hydrogen storage and transportation are the main problems that limit their applications. The fuel crossover problem of methanol and its own toxicity are the biggest shortcomings of DMFCs. DFAFC is a promising alternative to DMFCs due to its higher power density, lower fuel crossover, higher energy efficiency and higher electromotive force. Formic acid electro-oxidation (FAO), as the anode reaction of formic acid fuel cells, largely determines its operating efficiency. The currently recognized formic acid oxidation mechanisms include direct oxidation pathways and indirect oxidation pathways. Metal Pt, which is widely used in fuel cell catalysts, is expensive and has poor resistance to CO poisoning, which limits its large-scale application in DFAFC. The oxidation reaction of Pd-based catalysts to formic acid is mainly through a direct route[3]. Therefore, Pd-based catalysts are more suitable for formic acid fuel cells than Pt-based catalysts. However, the accumulation of CO_{ads} species on the active site of Pd will lead to undesirable stability[4].

An effective way to improve the performance of the catalyst is to select a suitable support material. The support not only affects the nucleation and growth process of the metal precursor, but also the size, valence and stability of the produced metal NPs can be further affected by the support material. Among them, carbon materials have the characteristics of large specific surface area, easy functionalization, low cost, and easy availability, making them the most promising catalyst support materials. Carbon materials such as carbon black[5], carbon nanotubes[6], and graphene[7] are widely used in the research of Pd-based catalysts. In addition, heteroatom doping (N, P, S, B, etc.) can optimize the surface structure and electronic properties of carbon materials[8-11]. The supports with improved physical and chemical properties can adjust the electronic state of the Pd surface through the strong interaction of the metal and support, thereby improving the catalytic activity and durability of Pd.

In recent years, nitrogen-doped carbon materials have been widely used as support for metal catalysts and have shown excellent electrocatalytic performance. Graphite carbon nitride (g-C_3N_4) is one of the promising materials among carbon-based materials which has a stacked graphene-like two-dimensional structure. It exhibits a large number of nitrogen coordination sites which is beneficial for the anchoring of metal NPs. The metal/semiconductor NPs supported by g-C_3N_4 have been proven to be effective composite materials in the fields of photocatalysis [12], organic catalysis [13], and electrochemical applications [14]. However, the electrochemical performance of g-C_3N_4 is not ideal due to its low conductivity [15]. In order to overcome this shortcoming, it is necessary to explore the possibility of combining g-C_3N_4 with carbon materials with good conductivity to obtain new support materials that have special electrochemical catalytic properties. Zhang [16] et al. prepared a composite of graphene oxide and graphite phase carbon nitride material supported palladium catalyst, which showed better catalytic activity and stability than Pd/rGO and commercial Pd/C in the oxidation reaction of formic acid and methanol. The performance improvement is attributed to the synergistic effect of rGO

and g-C_3N_4. The rGO makes up the shortcomings of poor conductivity of g-C_3N_4. At the same time, g-C_3N_4 brings more metal anchor points to the composite, thereby increase the dispersion of the catalyst active center and improve the catalytic activity. Moreover, the presence of g-C_3N_4 strengthens the corrosion resistance of the carbon support in acidic media, thus improving the stability of the catalyst.

Studies have shown that the doping of heteroatoms has been considered an effective way to adjust the electronic properties of g-C_3N_4. So far, g-C_3N_4 materials doped with heteroatoms such as B, P, S and F have been used in many fields such as electrocatalysis and photocatalysis [17-20]. However, there are few reports on the use of heteroatom-doped g-C_3N_4 as the metal Pd catalyst support. Here, this paper uses the composite of P-doped g-C_3N_4 and carbon black as the support to prepare a new type of Pd catalyst and applied it to the study of FAO.

2. EXPERIMENTAL DETAILS

2.1 Synthesis of C-g-C_3N_4 and C-PCN-X

700 mg of Vulcan XC-72 carbon black and 300 mg of melamine were mixed in 20 ml of deionized water. After ultrasonically dispersed for 1 hour, the suspension was continuously stirred and heated to 90℃ in a magnetic stirrer, then it was placed in a vacuum oven at 80℃ until the moisture is completely volatilized. After grinding, a homogeneous mixture of melamine and carbon black is obtained. This mixture was placed in a tube furnace in a nitrogen atmosphere, heated to 550℃ at a heating rate of 3℃/min and kept for 2h. After it was naturally cooled to room temperature, a carbon nitride/carbon black composite material was obtained, marked as C-g-C_3N_4. Phosphoric acid is introduced into the above mixture system to prepare phosphorus-doped carbon nitride/carbon black composite. Vulcan XC-72 carbon black (700 mg), melamine (300 mg) and a certain amount of phosphoric acid are mixed and dispersed in 20 ml deionized In the water. The mass ratio of phosphoric acid to melamine added is 1:10, 1:5, 1:1. The subsequent preparation process of C-PCN is the same as C-g-C_3N_4, and the prepared composite material is labeled as C-PCN-X (X=0.1, 0.2, 1).

2.2 Synthesis of Pd/C-g-C_3N_4 and Pd/C-PCN-X

In this experiment, a microwave-assisted polyol reduction method was used to prepare the catalysts. The specific experimental steps are as follows: 40 mg of support powder, 1.88 ml of 0.05 M $PdCl_2$ solution and 40 ml of ethylene glycol solution were added into a 100 ml three-necked flask, ultrasonically disperse for 10 minutes, and then slowly added 1mol/L NaOH/ethylene glycol solution dropwise until the pH of the above solution is 10. Continue to stir for 1 hour, the suspension was heated in a microwave synthesizer at a power of 600 W and a intermittent mode of 10 s-on/10 s-off for 7 cycles until the temperature of the solution reaches 130℃. After it cools naturally, 0.2 mol/L HCl solution was added dropwisely to adjust its pH to 3. This step accelerates the deposition rate of Pd NPs on the carrier. Finally, the above suspension was filtered, washed, and dried under vacuum oven for 4 hours. The resulting catalysts were labeled as Pd/C-g-C_3N_4, Pd/C-PCN-0.1, Pd/C-PCN-0.2 and Pd/C-PCN-1.

Pd/Vulcan XC-72 carbon black (Pd/C) catalyst was also prepared in the same way for comparison. The loading of Pd metal in all samples is 20 wt%.

2.3 Characterizations of catalysts

The crystal structure of the prepared catalysts were investigated by X-ray diffraction (XRD, Bruker D8 diffractometer). Scanning electron microscopy (SEM, JEOL 7800F) was used to record the surface morphology of the Pd/C and Pd/C-PCN-0.2 catalysts. The particle size distribution of the catalysts was measured by transmission electron microscopy (TEM, JEM-2100F). The chemical states of the elements in catalysts was analyzed by X-ray photoelectron spectra (XPS, VG Multilab 2000 spectrometer).

2.4 Electrochemical measurements

All electrochemical measurements of catalysts were performed with an electrochemical work station (CHI660E). A standard three-electrode electrochemical cell was used, including a glassy carbon electrode as the working electrode, a saturated calomel electrode (SCE) as the reference electrode, and a platinum wire as the counter electrode. The working electrode was prepared with the following procedure: a glassy carbon electrode was polished aluminum oxide powder and ultrasonically cleaned in ethanol and pure water, respectively. A certain amount of catalyst was dispersed ultrasonically in alcohol containing 0.5 wt% Nafion solution. About 4.0 μL of the above dispersed solution was scattered uniformly on a polished glassy carbon electrode. The working electrode was finished after drying at room temperature. The mass of Pd on the electrode is ca. 8 μg.

For CO stripping tests, the CO adsorption onto the catalyst was conducted at a potential of 0.2 V (versus SCE) in the 0.5 M H_2SO_4 solution with bubbling of 99.95% CO for 30 min. After purging pure nitrogen to release excess CO in the electrolyte, the stripping voltammograms were measured as a scan rate of 50 mV s^{-1}. Electrocatalytic activities of catalysts were evaluated by cyclic voltammograms (CV) in the HCOOH/H_2SO_4 solution after bubbled by pure N_2. The potential window of CV was from −0.2 V to 0.8 V (versus SCE) with a scanning rate of 50 mV s^{-1}. The stability of the catalysts was examined by chronoamperometry (CA), which were executed at a fixed potential of 0.1 V (versus SCE) in the HCOOH/H_2SO_4 solution for 1 h. All the tests were performed at room temperature.

3. RESULTS AND DISCUSSION

Figure 1 shows the XRD patterns of Pd/C, Pd/C-g-C_3N_4 and Pd/C-PCN-X catalysts. The peak at 2θ=25° belongs to C (002) crystal plane in these catalysts. Since the diffraction peak of g-C_3N_4 is covered by the broad peak of the C (002) crystal plane, it is impossible to distinguish the diffraction peak of g-C_3N_4 alone, which is consistent with the results reported by Qian [21] et al. The peaks at 2θ=40.1°, 46.7° and 68.1° are attributed to the diffraction peaks of metallic Pd, corresponding to the (111), (200) and (220) crystal planes of face-centered cubic structure Pd, respectively. As compared with Pd/C, the

diffraction peaks of Pd crystal planes of Pd/C-g-C_3N_4 and Pd/C-PCN-X catalysts have no obvious shift, which confirms that the introduction of carbon nitride has almost no effect on the crystal structure of Pd.

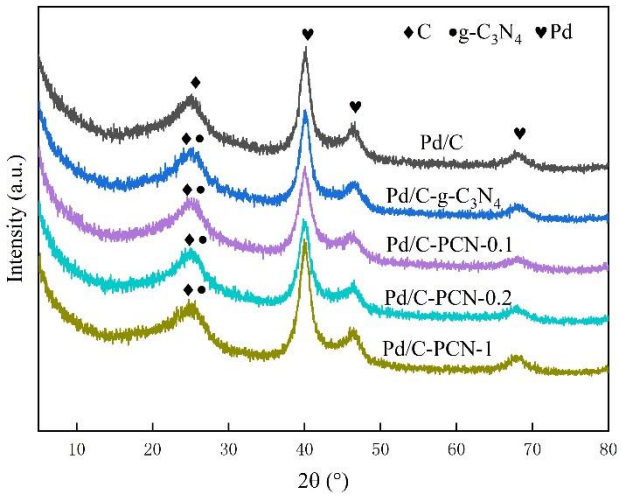

Figure 1. XRD patterns of Pd/C, Pd/C-g-C_3N_4, Pd/C-PCN-0.1, Pd/C-PCN-0.2 and Pd/C-PCN-1 catalysts.

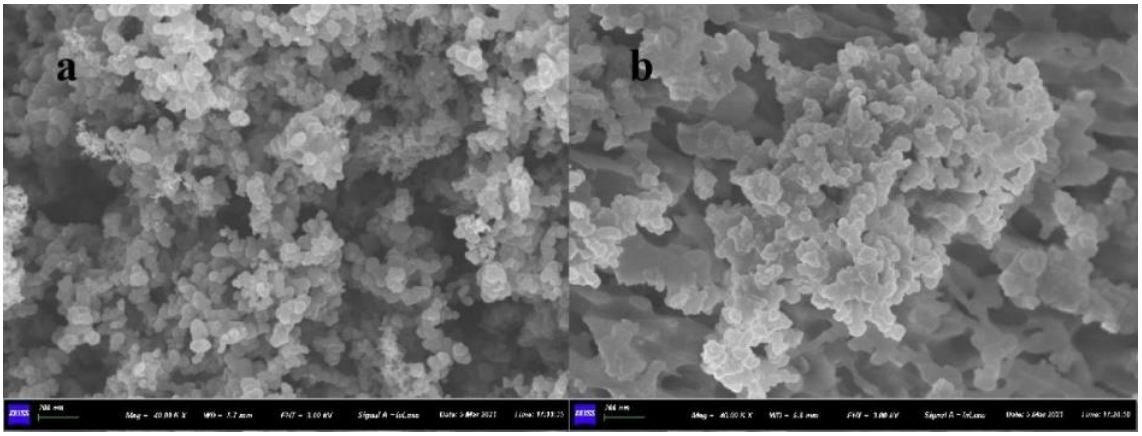

Figure 2. SEM spectra of Pd/C (a) and Pd/C-PCN-0.2 (b) catalysts.

Figure 2 shows the SEM spectra of Pd/C (a) and Pd/C-PCN-0.2 (b) catalysts. It can be seen that Vulcan XC-72 carbon black is a stacked spherical porous structure, and Pd/C-PCN-0.2 demonstrates a three-dimensional structure assembled from spherical carbon black and planar carbon nitride.

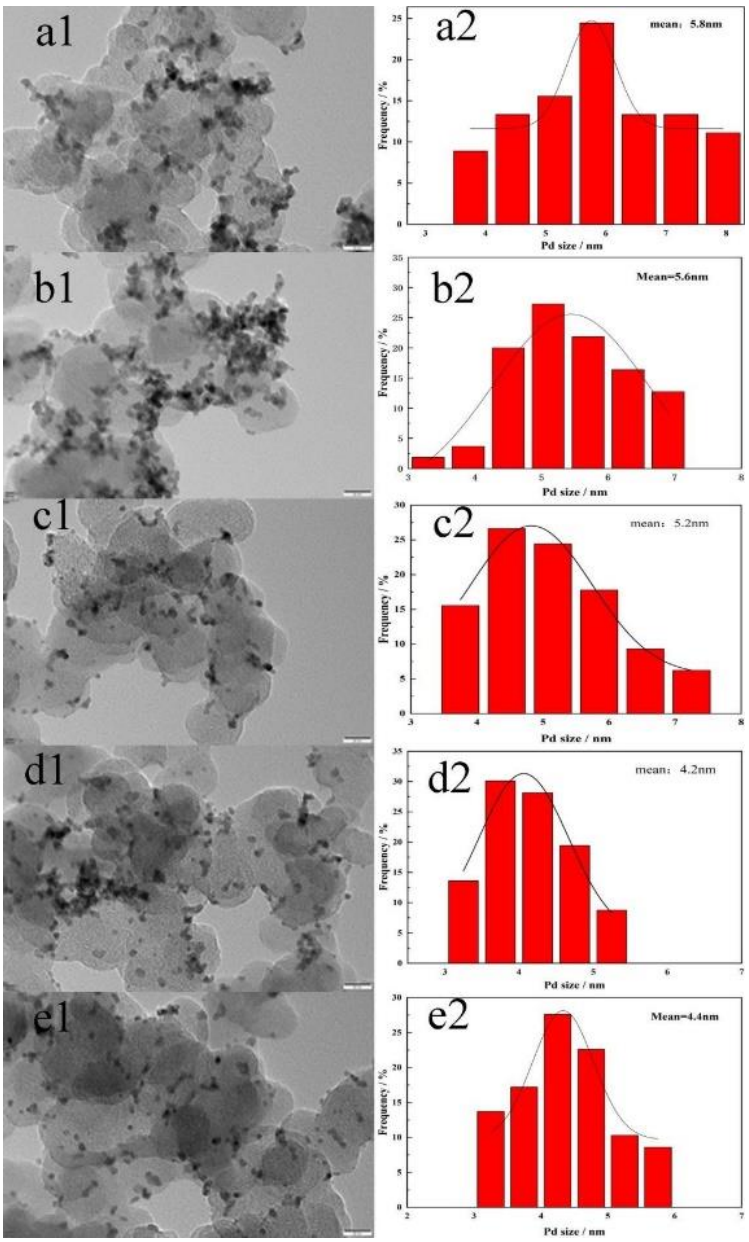

Figure 3. Typical TEM images and corresponding particle size distribution histograms of Pd/C (a1 and a2), Pd/C-g-C_3N_4 (b1 and b2), Pd/C-PCN-0.1 (c1 and c2), Pd/C-PCN-0.2 (d1 and d2) and Pd/C-PCN-1(e1 and e2) catalysts.

Figure 3 is the TEM spectra of Pd/C, Pd/C-g-C_3N_4 and Pd/C-PCN-X catalysts and their corresponding particle size distribution histograms. The average particle size of Pd particles in Pd/C, Pd/C-g-C_3N_4, Pd/C-PCN-0.1, Pd/C-PCN-0.2 and Pd/C-PCN-1 catalysts obtained from the statistical results of the histograms are 5.8, 5.6, 5.2, 4.2 and 4.4 nm, respectively. It can be seen that the introduction of carbon nitride is attribute to reduce the size of Pd NPs. Among the synthesized catalysts, the Pd/C-PCN-0.2 exhibits the smallest average particle size and the narrowest particle size distribution range. It can be due to the strong complexing ability of N atoms in carbon nitride to Pd ions, which facilitates the anchoring of the support to the metal during the reduction of Pd ions, thereby improving the dispersibility of Pd NPs.

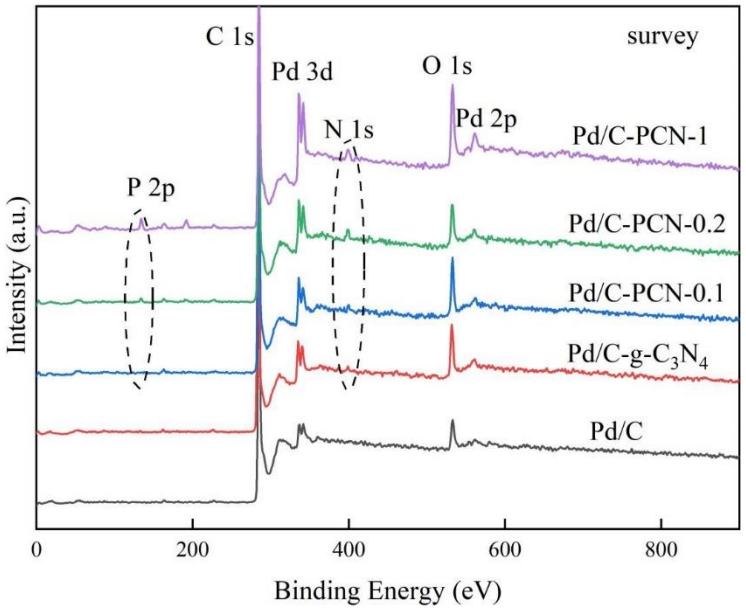

Figure 4. XPS survey spectra of Pd/C, Pd/C-g-C_3N_4, Pd/C-PCN-0.1, Pd/C-PCN-0.2 and Pd/C-PCN-1.

XPS technique was used to analyse the element composition and chemical state of the catalysts. Figure 4 is the XPS survey spectrum of Pd/C, Pd/C-g-C_3N_4 and Pd/C-PCN-X catalysts. The Pd/C-PCN-X is mainly composed of 5 elements: C, N, O, P and Pd. Table 1 lists the content of N and P elements in the catalysts. It can be seen that although the same amount of nitrogen source (melamine) of Pd/C-PCN-0.1, Pd/C-PCN-0.2 and Pd/C-PCN-1 catalysts was added during the preparation process, the nitrogen content in the catalysts increased with the increase of phosphorus source. It confirms that the presence of phosphorus can reduce the loss of nitrogen during the calcination process [22].

Table 1 The content of N and P elements in Pd/C-g-C_3N_4, Pd/C-PCN-0.1, Pd/C-PCN-0.2 and Pd/C-PCN-1 catalysts obtained from XPS

Catalysts	N (at%)	P (at%)
Pd/C-g-C_3N_4	2.19	--
Pd/C-PCN-0.1	3.09	0.51
Pd/C-PCN-0.2	3.68	1.52
Pd/C-PCN-1	3.77	4.95

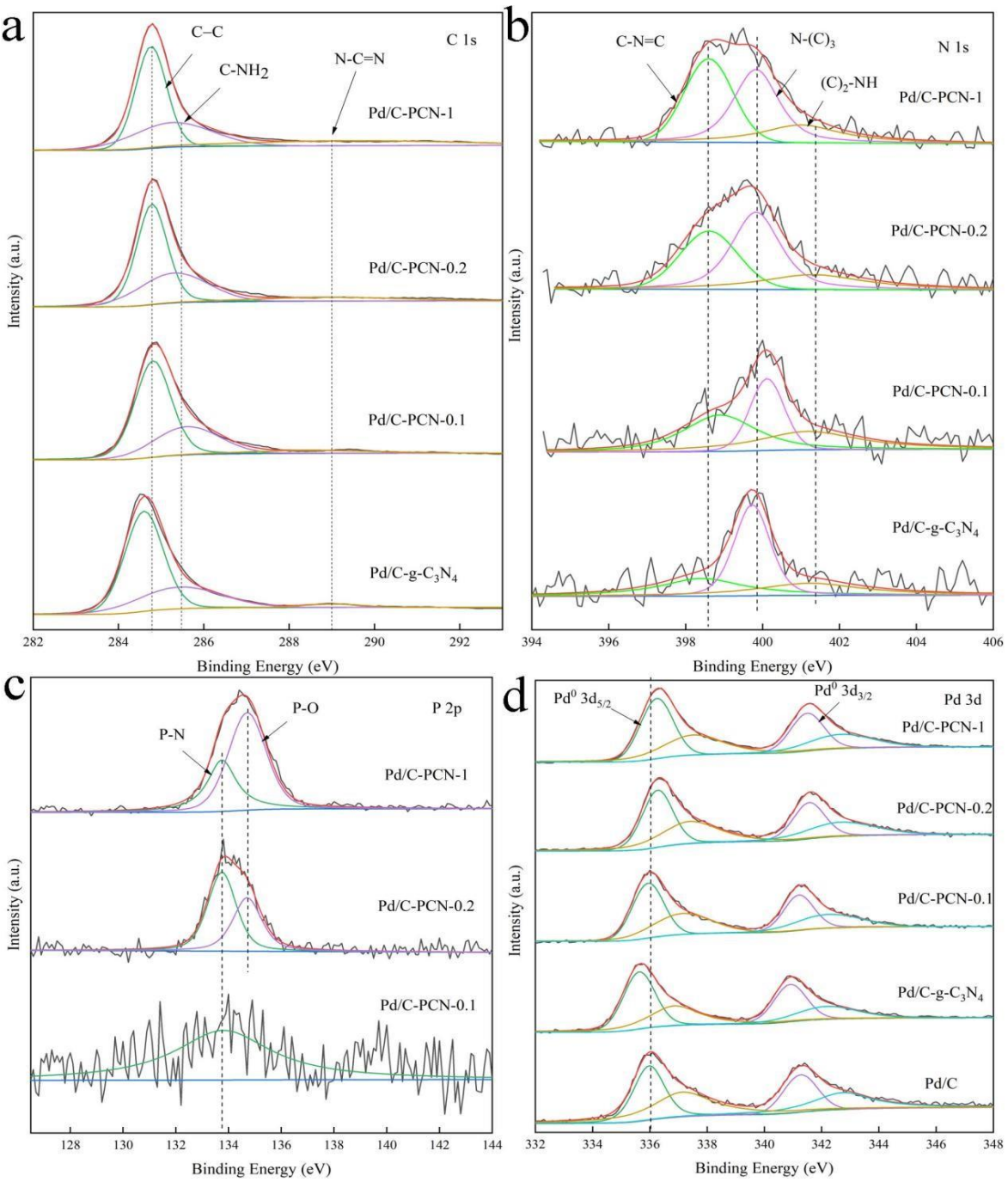

Figure 5. XPS spectra of C 1s (a) and N 1s (b) of Pd/C-g-C_3N_4, Pd/C-PCN-0.1, Pd/C-PCN-0.2 and Pd/C-PCN-1 catalysts, P 2p (c) of Pd/C-PCN-0.1, Pd/C-PCN-0.2 and Pd/C-PCN-1 catalysts and Pd 3d (d) of Pd/C, Pd/C-g-C_3N_4, Pd/C-PCN-0.1, Pd/C-PCN-0.2 and Pd/C-PCN-1 catalysts.

As shown in Figure 5(a), the signal peak of C 1s of Pd/C-PCN-0.2 catalyst can be divided into 3 peaks, corresponding to the sp2 hybridized C-C (284.8 eV), C-NH_2 (285.3 eV) and NC=N (288.9 eV) in C_3N_4 [23-25]. Figure 5(b) is the N 1s spectrum which forms of three nitrogen species. The peak at 398.8 eV is assigned to CN=C in the triazine ring, while as the peak at 399.5 eV belongs to the nitrogen atom bridging the inter-triazine ring (N-C3), the peak centred at 401.1eV is attributed to the amino nitrogen (NH) at the edge of g-C_3N_4 [26, 27]. As presented in figure 5(c), the P 2p spectra of Pd/C-PCN-0.2 and Pd/C-PCN-1 can be divided into two peaks at 133.7 and 134.7 eV, respectively. Since the binding

energies of P 2p in the P-C, P-N and P-O bonds are about 131, 133 and 135 eV, respectively [28], it can be reasonably speculated that the introduced P element exists in the g-C_3N_4 structure in the form of P-N and P-O bonds. In addition, P-N is not detected in the N 1s spectrum of Pd/C-PCN-X, which is due to the rather lower concentration of P-N in comparison with the bond between N and C. The analysis of the relative content of P-N and P-O in the Pd/C-PCN-0.1, Pd/C-PCN-0.2 and Pd/C-PCN-1 catalysts shows that only P-N is contained in Pd/C-PCN-0.1. Pd/C-PCN-0.2 contains 57.8% of P-N and 42.2% of P-O. This is due to the increase in the introduction of phosphorus, which leads to a part of P in the form of PO_4^{3-}[29-31]. It also explains that the more concentration of P-O (65.2%) in Pd/C-PCN-1 compares with the concentration of P-N. In summary of the structural analysis, the P element exists in the form of P-N and P-O bonds. The former is attributed to the replacement of C by P in the g-C_3N_4 structure, and the latter is ascribed to the incomplete decomposition of phosphoric acid. Figure 5(d) shows the Pd 3d XPS spectra of Pd/C, Pd/C-g-C_3N_4 and Pd/C-PCN-X catalysts. The XPS signal peak of Pd 3d can be deconvolved into two pairs of peaks, corresponding to the metal state of Pd^0 and the oxidation state of Pd^{2+}. For example, the peaks at 336.3eV, 337.4eV, 341.6eV and 342.7eV correspond to Pd^0 $3d_{5/2}$, Pd^{2+} $3d_{5/2}$, Pd^0 $3d_{3/2}$ and Pd^{2+} $3d_{3/2}$ of Pd/C-PCN-0.2 catalyst, respectively.

Binding energy of Pd species of each catalyst and its shift compared to Pd/C is listed in Table 2. Compared with Pd/C, the binding energy of Pd^0 $3d_{5/2}$ in the Pd/C-g-C_3N_4 catalyst is negatively shifted by 0.4 eV. It is owing to the interaction between Pd NPs and C-g-C_3N_4 composite support. In this hybrid catalyst system, Pd acts as an electron acceptor from g-C_3N_4 which leads to an increase in the density of Pd 3d electron cloud, thus showing a negative shift in the binding energy of Pd^0 3d. This phenomenon is consistent with the results reported by Zhang et al. [16]. However, Pd/C-PCN-0.2 and Pd/C-PCN-1 catalysts exhibit a positively shifted Pd 3d binding energy compared to Pd/C, which indicates that P doping changes the electronic structure of g-C_3N_4, varying the Pd as an electron donor when interacting with C-PCN support. It can be concluded that the positive shift of the binding energy of the Pd species is related to the phosphorus element. When the Pd NPs interact with the support, electrons are transferred to the phosphorus, resulting in a decrease in the density of the Pd 3d electron cloud and a positive shift of the binding energy.

Table 2 Binding Energy (BE) of Pd 3d of Pd/C, Pd/C-g-C_3N_4, Pd/C-PCN-0.1, Pd/C-PCN-0.2 and Pd/C-PCN-1 catalysts and its shift compare to Pd 3d of Pd/C.

Catalysts	Species	Binding Energy	BE Shift（eV)
Pd/C	$Pd^0 3d_{3/2}$	341.27	0
	$Pd^0 3d_{5/2}$	335.97	0
Pd/C-g-C_3N_4	$Pd^0 3d_{3/2}$	340.91	-0.36
	$Pd^0 3d_{5/2}$	335.63	-0.34
Pd/C-PCN-0.1	$Pd^0 3d_{3/2}$	341.21	-0.06
	$Pd^0 3d_{5/2}$	335.94	-0.03
Pd/C-PCN-0.2	$Pd^0 3d_{3/2}$	341.56	0.28
	$Pd^0 3d_{5/2}$	336.27	0.3
Pd/C-PCN-1	$Pd^0 3d_{3/2}$	341.50	0.23
	$Pd^0 3d_{5/2}$	336.24	0.27

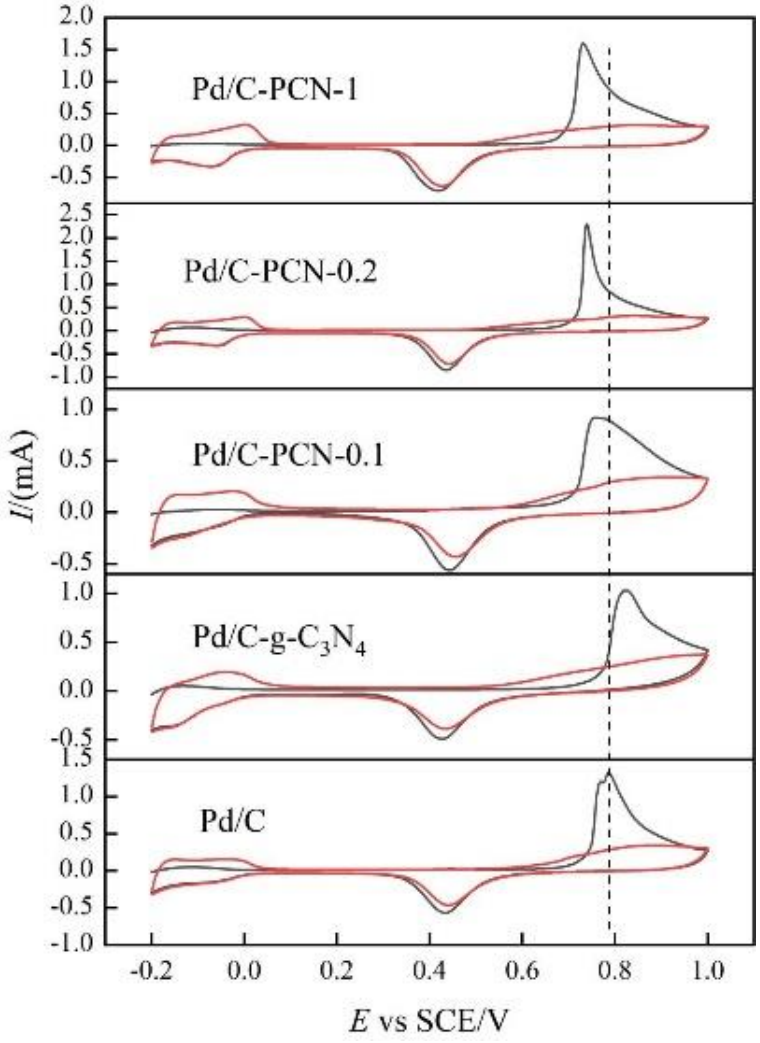

Figure 6. CO-stripping curves of Pd/C, Pd/C-g-C_3N_4, Pd/C-PCN-0.1, Pd/C-PCN-0.2 and Pd/C-PCN-1 catalysts in 0.5 M H_2SO_4 solution at a scan rate of 50 mV s^{-1}.

CO-stripping test was used to analyze the anti-CO poisoning ability of the prepared catalysts and calculate its electrochemical specific surface area (ECSA). As shown in figure 6, the CO oxidation peak potentials of Pd/C, Pd/C-g-C_3N_4, Pd/C-PCN-0.1, Pd/C-PCN-0.2 and Pd/C-PCN-1 catalysts are 787, 824, 759, 731 and 734 mV, respectively. It can be seen that the CO oxidation peak of Pd/C-g-C_3N_4 catalyst is positively shifted compared to Pd/C, while the CO oxidation peak on Pd/C-PCN-X is negatively shifted to different degrees compared to Pd/C. It indicates that the adsorption strength of CO_{ads} on Pd/C-g-C_3N_4 catalyst is stronger than that on Pd/C, while the adsorption strength on Pd/C-PCN-X catalyst is weaker than that on Pd/C. As described in XPS analysis, the Pd 3d electron cloud density in the Pd/C-PCN-X catalyst decreases, which will weaken the adsorption of CO_{ads} on the Pd surface, thereby enhancing the ability to resist CO poisoning. On the contrary, the ability of Pd/C-g- C_3N_4 catalyst to resist CO poisoning is weakened.

The ECSA of the catalysts were calculated using the following formula, and the results are shown in Table 3.

$$\mathrm{ECSA}\,(\mathrm{m^2\ g^{-1}}) = \frac{\mathrm{Q_{CO}}\ (\mu\mathrm{C})}{420\ (\mu\mathrm{C\ cm^{-2}})}\frac{100}{m\ (\mu\mathrm{g})}$$

Q_{CO} denotes the columbic charge of CO_{ads} oxidation, m represents the catalyst mass on the electrode, columbic charge required for the oxidation of CO_{ads} monolayer is assumed as 420 μC cm^{-2}, according to the literature [32].

Table 3 Electrochemical data for CO-stripping, cyclicvoltammetry and chronoamperometry of Pd/C-g-C_3N_4, Pd/C-PCN-0.1, Pd/C-PCN-0.2, Pd/C-PCN-1 and Pd/C catalysts.

Catalysts	Pd/C-g-C_3N_4	Pd/C-PCN-0.1	Pd/C-PCN-0.2	Pd/C-PCN-1	Pd/C
ECSA ($m^2\ g^{-1}$)	53	56	65	62	49
Peak potential (mV)	824	759	734	731	787
Mass current (A/g)	497	571	771	645	358
I_{3600}/I_{10}	3.14%	5.93%	6.68%	5.44%	2.87%

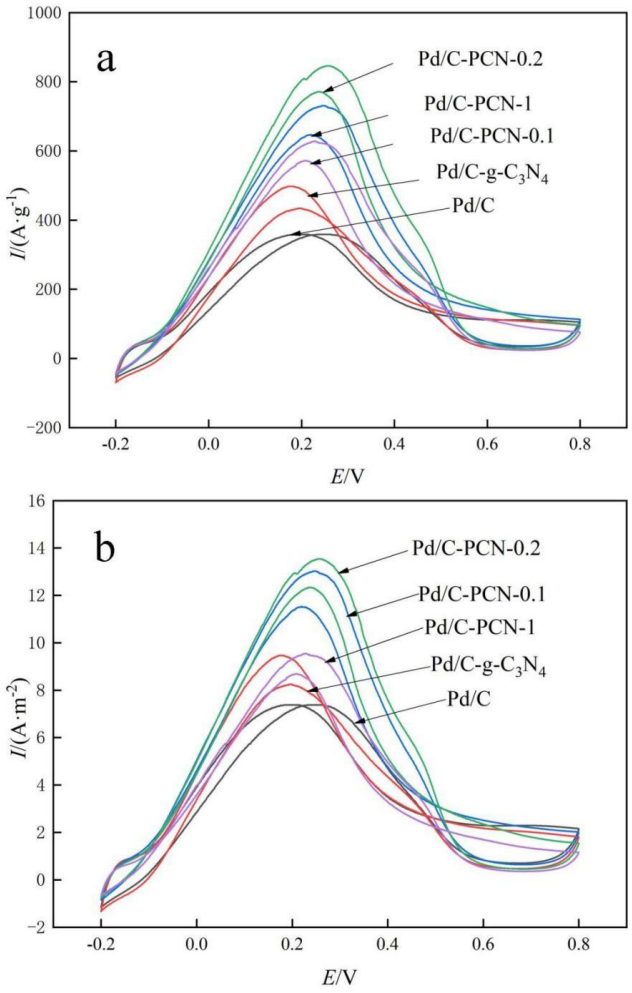

Figure 7. CV curves of Pd/C, Pd/C-g-C_3N_4, Pd/C-PCN-0.1, Pd/C-PCN-0.2 and Pd/C-PCN-1 catalysts in 0.5 M H2SO4 + 0.5 M HCOOH solution with a scan rate of 50 mV s^{-1}. The currents were normalized to the (a) mass currents and (b) specific currents.

Cyclic voltammetry was used to evaluate the activity of the prepared catalysts for the FAO. As shown in figure 7(a), the oxidation peak potential of the catalysts for formic acid reach around 0.2 V, the Pd/C-g-C_3N_4 catalyst reaches the current peak at a lower potential than other catalysts, indicating that formic acid is more likely to be oxidized on the surface of the Pd/C-g-C_3N_4 catalyst. This may be due to the Pd/C-g-C_3N_4 catalyst has a strong adsorption effect on the active intermediate of the formic acid oxidation process, and accelerates the first step of formic acid oxidation process. However, the strong adsorption capacity of the CO_{ads} and other poisonous intermediates on the catalyst hinder the further improvement of the catalytic activity. The peak currents of the prepared catalysts for the oxidation of formic acid follows the following order: Pd/C-PCN-0.2>Pd/C-PCN-1>Pd/C-PCN-0.1>Pd/C-g-C_3N_4>Pd/C. The catalytic activity of Pd/C-PCN-0.2 (771 A/g) is the highest, reaching 2.15 times that of Pd/C (358 A/g). As shown in figure 7(b), the specific activities of the Pd/C, Pd/C-g-C_3N_4, Pd/C-PCN-0.1, Pd/C-PCN-0.2 and Pd/C-PCN-1 catalysts calculated according to the ECSA are 7.38, 9.46, 11.53, 12.34 and 8.68 $A \cdot m^{-2}$, respectively. The similar electrocatalysts reported in the literature are listed in Table 4 for comparison. The excellent catalytic performance of C-PCN-0.2 can be attributed to the uniform dispersion of Pd on the support, which increases the number of catalytic active sites. Secondly, the introduction of nitrogen and phosphorus in the carrier changes the electronic structure of the Pd surface, and the doping amount of phosphorus optimizes the electronic structure of the Pd surface and improves its better adsorption capacity for reactive species and desorption capacity of poisonous intermediates.

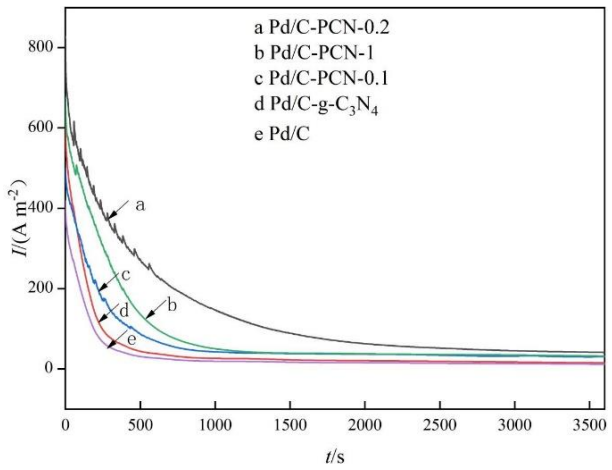

Figure 8. Chronoamperometric curves of Pd/C, Pd/C-g-C_3N_4, Pd/C-PCN-0.1, Pd/C-PCN-0.2 and Pd/C-PCN-1 catalysts at 0.1 V.

Chronoamperometry was used to evaluate the stability of the prepared catalysts for the FAO. The experiments were conducted at a constant potential of 0.1 V in 0.5 M H_2SO_4/HCOOH solution for 3600s. As shown in figure 8, the initial current of the catalysts is basically consistent with the results of the CV curve. The current density of the catalysts have just begun to decay rapidly. As the reaction progressed, the decay of the current density gradually becomes flat. This is due to the adsorption of CO_{ads} on the Pd nanoparticles produced by the formic acid oxidation process, which causes the active centers to be

shielded, and the corrosion of carbon materials and the agglomeration of palladium NPs caused by long-term work under acidic conditions. After 3600s, the current densities of the Pd/C, Pd/C-g-C_3N_4, Pd/C-PCN-0.1, Pd/C-PCN-0.2 and Pd/C-PCN-1 catalysts were 11, 15, 30, 41 and 32 A/g, respectively. The ratio of the current I_{3600} in the reaction time of 3600s and the current I_{10} in the reaction time of 10s was used to evaluate the stability of the catalyst. The calculated I_{3600}/I_{10} of Pd/C, Pd/C-g-C_3N_4, Pd/C-PCN-0.1, Pd/C-PCN-0.2 and Pd/C-PCN-1 catalysts are 2.87%, 3.14%, 5.93%, 6.68% and 5.44%, respectively. The results show that the Pd/C-g-C_3N_4 and Pd/C-PCN-X catalysts have improved the electrocatalytic oxidation stability of FAO. The enhanced stability of the Pd/C-PCN-X catalysts is due to the weak adsorption strength of CO_{ads} on the Pd surface, which is easy to be oxidized, thereby exposing more active centers. The reason why the stability of Pd/C-g-C_3N_4 is better than that of Pd/C catalyst may be that the introduction of g-C_3N_4 enhances the corrosion resistance of carbon black in acidic environments. In addition, the anchoring effect of N element on Pd improves the interaction of metal carriers. It inhibits the agglomeration of Pd nanoparticles.

Table 4 Summary of the literature data on ECSA and mass activity of formic acid oxidation obtained from similar electrocatalysts and comparison with this work.

catalysts	electrolyte solution	ECSA (m^2 g^{-1})	mass activity (A/g)	reference
Pd/PCNTs	0.5MHCOOH+0.5MH_2SO_4	72	694	[9]
Pd/g-C_3N_4-rGO-2	0.5MHCOOH+0.5MH_2SO_4	107	1610	[16]
Pd/P-C-800	0.5MHCOOH+0.5MH_2SO_4	40	775	[33]
Pd/NP-coal-CFs	0.5MHCOOH+0.5MH_2SO_4	87	536	[34]
Pd/MMT-CN_x	0.5MHCOOH+0.5MH_2SO_4	22	763	[35]
Pd/C-PCN-0.2	0.5MHCOOH+0.5MH_2SO_4	65	771	this work

4. CONCLUSIONS

In short, a mixture of carbon black, melamine, and phosphoric acid were calcined in one-step to obtain a phosphorus-doped carbon nitride and carbon black composites and used as a Pd catalyst support. When the mass ratio of phosphoric acid and melamine added was 1:5, the corresponding Pd/C-PCN-0.2 catalyst showed the best electrocatalytic performance. TEM result shows that it has the narrowest range of particle size distribution and the smallest average particle size. The peak current density of Pd/C-PCN-0.2 to FAO is 771 A/g, which is 2.15 times that of Pd/C. The Pd/C-PCN-0.2 tested for a long time still exhibits higher activity than other catalysts. Its current density at 3600s is 41 A/g, which is 3.7 times that of the Pd/C catalyst. Moreover, the CO oxidation peak of Pd/C-PCN-0.2 catalyst was negatively shifted by 56 mV compared to Pd/C, indicating its excellent resistance to CO poisoning. The increase in the activity and stability of the Pd/C-PCN-X catalysts is attributed to the more uniformly dispersed Pd NPs and the improved electronic structure of the Pd NPs. This is because the strong interaction between carbon black and phosphorus-doped carbon nitride composite and Pd not only improves the dispersibility of Pd, but also makes the Pd nanoparticles in the Pd/C-PCN-X catalyst show an electron-deficient state.

Therefore, it is difficult to combine with COOH intermediates that easily produce CO. The catalyst oxidizes formic acid through a direct route, which improves its catalytic activity and stability.

ACKNOWLEDGMENTS
This research was financially supported by the Natural Science Foundation of Hubei Province (Grant No. 2016CFA079), the Opening Fund of Key Laboratory of Green Chemical Process of Ministry of Education (No. GCP20190206) and Opening Fund (WKDM202106) from Key Laboratory of Hubei Province for Coal Conversion and New Carbon Materials (Wuhan University of Science and Technology).

References

1. G. W. Crabtree, M. S. Dresselhaus and M. V. Buchanan, *The hydrogen economy*. *Phys Today,* 57 (2004) 39-44.
2. Y. Wang, H. Liu, L. Wang, H. Wang, X. Du and F. Wang, *J Mater Chem A,* 1 (2013) 6839-48.
3. C. Rice, S. Ha, R. I. Masel, P. Waszczuk, A. Wieckowski and T. M. Barnard, *J. Power Sources,* 111 (2002) 83.
4. X. Yu and P. G. Pickup, *Electrochem. Commun.,* 11 (2009) 2012.
5. J. Y. Wang, Y. Y. Kang, H. Yang and W. B. Cai, *J. Phys. Chem. C,* 113 (2009) 8366.
6. R. D. Morgan, A. Salehi-khojin and R. I. Masel, *J. Phys. Chem. C,* 115 (2011) 19413.
7. J. Yang, C. G. Tian, L. Wang and H. G. Fu, *J. Mater. Chem.,* 21 (2011) 3384.
8. H. Jiang, L. Liu, K. Zhao, Z. Liu, X. S. Zhang and S. Z. Hu, *Electrochim. Acta,* 337 (2020) 135758.
9. Z. L. Xin, S. H. Wang, J. Wang, X. Huang, X. B. Ji, Y. Y. Yao and L. D. Shao, *Electrochem. Commun.,* 67 (2016) 26.
10. X. Zhang, X. Zhang, J. X. Zhu, C. S. Tiwary, Z. Y. Ma, H. J. Huang, J. F. Zhang, Z. Y. Lu, W. Huang and Y. P. Wu, *ACS Appl. Mater. Interf.,* 8 (2016) 10858.
11. Y. Yang, H. J. Huang, B. F. Shen, L. Jin, Q. G. Jiang, L.Yang and H. Y. He, *Inorg. Chem. Front.,* 7 (2020) 700.
12. T. Bhowmik, M. K. Kundu and S. Barman, *RSC Advances,* 5 (2015) 38760-38773.
13. M. K. Kundu, M. Sadhukhan and S. Barman, *Journal of Materials Chemistry B,* 3 (2015) 1289-1300.
14. T. Bhowmik, M. K. Kundu and S. Barman, *Acs Catalysis,* 6(2016) 1929-1941.
15. S. B. Yang, X. L. Feng, X. C. Wang, K. Müllen and Angew, *Chem. Int. Ed,* 50 (2011) 5339-5343.
16. W. Zhang, H. Huang, F. Li, K. Deng and X. Wang, *Mater. Chem. A,* 2 (2014) 19084-19094.
17. Y. P. Zhu, T. Z. Ren and Z. Y. Yuan, *ACS applied materials & interfaces,* 7 (2015) 16850-16856.
18. G. Liu, P. Niu and C. Sun, *Journal of the American Chemical Society,* 132 (2010) 11642-11648.
19. Y. Wang, Y. Di and M. Antonietti, *Chemistry of Materials,* 22 (2010) 5119-5121.
20. C. Liu, Y. Zhang and D. Fan, *Applied Catalysis B: Environmental,* 203 (2017) 465-474.
21. H. Qian, H. Huang, W. Xin, *Journal of Power Sources,* 275 (2015) 734-741.
22. C. H. Choi, S. H. Park and S. I. Woo, *Journal of Materials Chemistry,* 22 (2012) 12107-12115.
23. D. Xyab, T. B. Lin and C. Xz, *Applied Catalysis B: Environmental,* 244 (2019) 240-249.
24. Y. Yang, C. Zhang and D. Huang, *Applied Catalysis B: Environmental,* 245 (2019) 87-99.
25. W. Zhang, X. Li and X. Xu, *Journal of Materials Chemistry B,* 7 (2019) 233-239.
26. H. B. Fang, X. H. Zhang and J. Wu, *Applied Catalysis B: Environmental,* 225 (2018) 397-405.
27. S. Guo, Y. Tang and Y. Xi, *Applied Catalysis B: Environmental,* 218 (2017) 664-671.
28. S. Hu, L. Ma and J. You, *Applied Surface Science,* 311 (2014) 164-171.
29. X. She, L. Liu and H. Ji, *Applied Catalysis B: Environmental,* 187 (2016) 144-153.
30. S. Ou é draogo, B. Chouchene and C. Desmarets, *Applied Catalysis A: General,* 563 (2018) 127-

136.
31. P. Qiu, C. Xu and H. Chen, *Applied Catalysis B Environmental,* 206 (2017) 319-327.
32. X. Zhao, J. B. Zhu, L. Liang, C. P. Liu, J. H. Liao and W. Xing, *J. Power Sources,* 210 (2012) 392.
33. J. D. Li, Q. F. Tian, S. Y. Jiang, Y. Zhang and Y. X. Wu, *Electrochim. Acta*, 213 (2016) 21.
34. M. R. Lou, R. Y. Wang, J. Zhang, X. C. Tang, L. X. Wang, Y. Guo, D. Z. Jia, H. L. Shi, L. L. Yang, X. C. Wang, Z. P. Sun, T. Wang and Y. D. Huang, *ACS Appl. Mater. Interfaces,* 11 (2019) 6431.
35. Q. F. Tian, W. Chen, L. F. Zhang, F. Zhang and Y. X. Wu, *Ionics,* 21 (2014) 1693.